Morphological Feature Extraction Based on Multiview Images for Wear Debris Analysis in On-line Fluid Monitoring

Tonghai Wu, Yeping Peng, Shuo Wang, Feng Chen, Ngaiming Kwok & Zhongxiao Peng

Published online: 10 Aug 2016.

Submit your article to this journal ⤤

View related articles ⤤

View Crossmark data ⤤

Citing articles: 7 View citing articles ⤤

Morphological Feature Extraction Based on Multiview Images for Wear Debris Analysis in On-line Fluid Monitoring

Tonghai Wu[a], Yeping Peng[a,b], Shuo Wang[a], Feng Chen[a], Ngaiming Kwok[b], and Zhongxiao Peng[b]

[a]Key Laboratory of Education Ministry for Modern Design and Rotor-Bearing System, School of Mechanical Engineering, Xi'an Jiaotong University, Xi'an, P. R. China; [b]School of Mechanical and Manufacturing Engineering, The University of New South Wales, Sydney, New South Wales, Australia

ABSTRACT

Wear state is an important indicator of machinery operation condition that reveals whether faults have developed and maintenance should be scheduled. Among the available techniques, vision-based on-line monitoring of wear particles in the lubricant circuit is preferred, where three-dimensional particle characterizations can be obtained for wear mode analysis. This article presents the application of an imaging system that captures wear particles in lubricant flow and the development of image processing procedures for multiview feature extraction. In particular, a framework including background subtraction, object segmentation, and debris tracking was adopted. Particle features were then used in a comprehensive morphological description of wear debris. Experiments showed that the system is able to produce a feasible and reliable indication of wear debris characteristics for machine condition monitoring.

Introduction

Wear is one of the most inherent and noticeable phenomena in machines with components in contact and relative motion. The health status of a machine can therefore be investigated by monitoring the degree of wear on the components. However, this task often requires shutting down or disassembling the machine, thus imposing additional operation costs as well as loss of production. On the other hand, wear debris particles are produced during the wear process, and these particles can be an indicator of the morphology and degree of wear. Based on the fact that most machines have a lubrication system and wear debris particles are carried through the lubricant circuitry, on-line monitoring of wear particles is possible by securing a representative fluid sample for microscopic analysis, in particular, ferrography. This vision-based technique is very attractive because it is not necessary to interrupt the operation of the machine (Kumar, et al. (1); Wu, et al. (2); Wang and Wang (3)).

Ferrography as a vision-based technique that is regarded as an effective method for the estimation of wear particle concentration as well as their characteristics (Zhang, et al. (4); Wang, et al. (5); Li, et al. (6)). However, particle overlap is a commonly reported issue with ferrography, making it difficult to examine individual wear particles. Furthermore, because conventional ferrography makes use of only single-view images, 3D particle features cannot be conveniently provided. Thus, the necessary spatial information, such as surface roughness and particle thickness, is not available to fully study wear mechanisms and reveal wear conditions with better precision (Yuan, et al. (7)).

Research efforts have also been directed toward extracting particle features in 3D (Stachowiak and Podsiadlo (8); Tian, et al. (9); Yuan, et al. (10); Podsiadlo and Stachowiak (11)). Among these attempts, stereo scanning electron microscopy (Stachowiak, et al. (12)), laser scanning confocal microscopy (Peng, et al. (13); Peng and Tomovich (14)), and atomic force microscopy (Wang, et al. (15)) were developed to acquire wear debris contour and surface information. However, these methods either rely on a single view of static wear particles or require manual extraction, which is often time consuming.

Real-time wear debris imaging has been advanced using magnetic deposition sensors (Du and Zhe (16); Feng, et al. (17); Cao, et al. (18)) and flow-free sensors (Murali, et al. (19); Filicky, et al. (20)). Individual particles can be identified using magnetic deposition with on-line visual ferrography, but it is vulnerable to particle overlap and aggregation (Wu, et al. (21)). Although the LaserNet Fines system resolves this problem by employing a free flow cell (Spectro Inc. (22)), the extracted features are not comprehensive because a single-view image is used. In order to obtain a better description of wear characteristics, a method based on 3D multiple views was proposed (Dan (23)), where the particle volume could be estimated.

In order to realize on-line analysis of wear debris for machine condition monitoring, a new approach is proposed. In our previous work (Peng, et al. (24), (25)), a video acquisition system was designed to capture dynamic images of moving particles. The purpose of this work was to develop a new solution to dynamically extract wear debris morphological features. The developed system adopts the visual ferrography principle and

---

incorporates the multiview strategy to extract 3D features of wear debris flowing in a lubricant circuit. Then with the use of background subtraction, moving object segmentation, detection, and tracking (Meijering, et al. *(26)*; Karasulu and Korukoglu *(27)*), multiview particles are identified and their 3D features are determined.

The remainder of the article is organized as follows. In the following section, the video system to acquire wear debris carried in lubrication fluid is presented. Procedures developed for moving particle segmentation, identification, and tracking are detailed next. The proposed particle characterization approach from multiview images is presented in the same section. The next section describes the experiment, different types of test sets of wear debris, and the resultant particle feature descriptors. The advantages of this proposed approach in comparison to existing methods are also discussed. The final section presents our conclusion.

Wear debris image acquisition system

It is recognized that key spatial features of particles, such as thickness, cannot be reliably provided by a single-view image (Peng and Tomovich *(14)*). Thus, multiview images are necessary to obtain a comprehensive description of a particle. To this end, a video acquisition system was designed to capture multiview images of wear particles when they are moving in a lubricant flow. The wear debris image acquisition system is depicted in Fig. 1.

For example, the imaging system is applied in capturing debris generated from gearbox wear. In order to obtain particle images from different viewing directions, a rectangular

lubricant flow path with sectional dimension of 6×0.2 mm^2 is used to achieve laminar flow. While wear particles are moving and rotating under the laminar condition, multiple views of particles can be captured from different directions using a video sensor. The sensor outputs a video stream at 50 fps. The video frames are transferred to a computer as input for further processing to extract particle features. Details of the developed wear debris identification and feature extraction techniques will be presented later.

Particle identification and tracking

An illustration of a series of particle images taken is shown in Fig. 2. As seen in the figure, the wear debris images were acquired in different views when particles were moving within the fluid flow. Thus, 2D morphological features of wear debris can be obtained by processing these images individually. By doing so, the on-line wear debris image analysis procedure is simplified to processing a set of multiple static images to acquire spatial information.

It can also be seen that there are often many particles appearing in one frame image, making it difficult to detect them. Furthermore, the same wear debris would appear in different shapes at changing locations and with various features in different images. A reliable and efficient particle tracking method therefore needs to be established before the wear features of the particle can be effectively extracted. A flowchart of the proposed approach is illustrated in Fig. 3.

As mentioned earlier, the image acquisition system captures video frames and inputs them to a computer software program. The developed image processing procedure serves two main
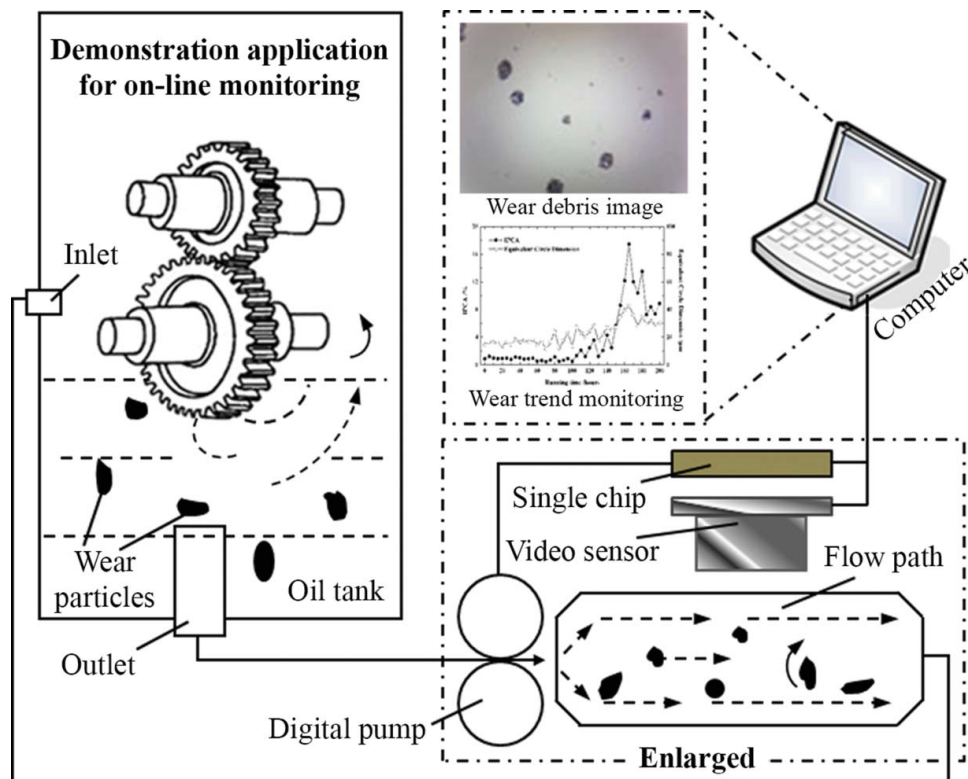

Figure 1. Principle of the proposed on-line wear debris image acquisition and monitoring system.
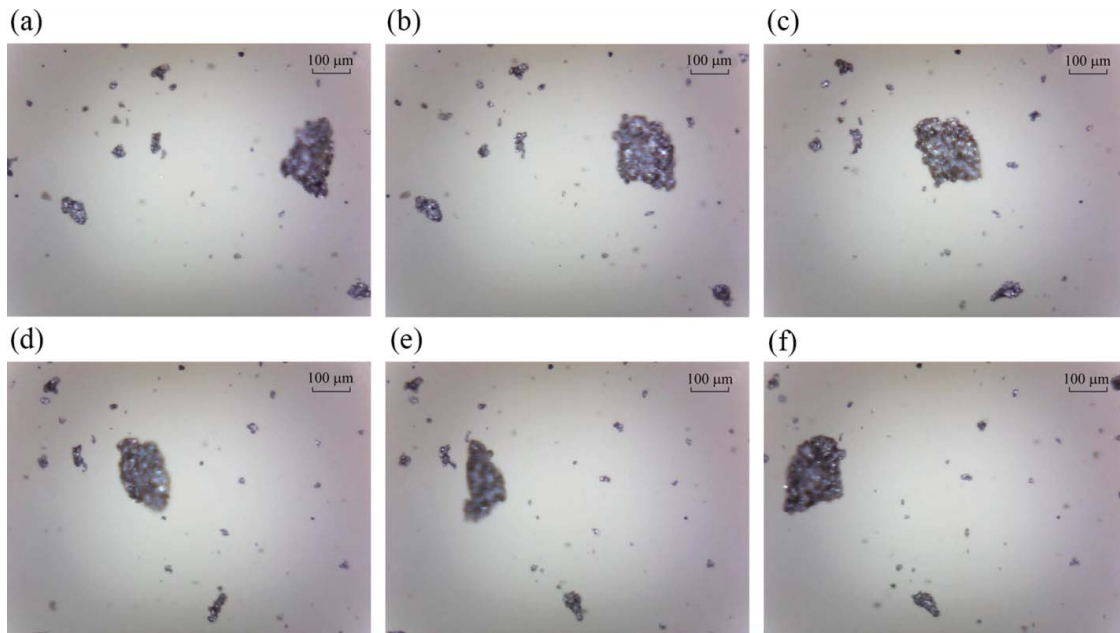
Figure 2. Series of wear debris image frames: (a) Frame 20, (b) Frame 40, (c) Frame 60, (d) Frame 80, (e) Frame 100, and (f) Frame 120.

purposes: to separate wear debris and to extract particle features. To achieve these objectives, a five-step procedure is adopted:

1. Conduct video sampling to obtain image frames using the video acquisition system (Wear debris image acquisition system section).
2. Update dynamic background with consistent frames in response to varied illumination (Dynamic background update section).
3. Segment target particle from dynamic background to obtain the wear debris of interest (Wear debris segmentation section).
4. Track wear debris with different appearances in different frames (Dynamic tracking of moving wear debris section).
5. Extract wear debris features with different views (Feature construction based on multiview images section).
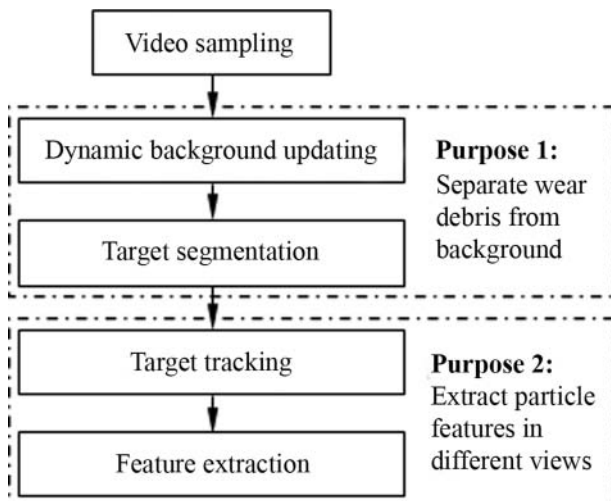

Figure 3. Flowchart of moving wear debris detection and tracking with multiple images in different views.

Dynamic background update

A captured image would contain a background with wear debris in the foreground. Separation of wear debris in a static image is relatively easily accomplished by utilizing differences in gray values between wear debris and the background. In order to obtain information on wear debris, object segmentation algorithms were considered. To this end, automatic thresholding (Zhang, et al. *(28)*) and background subtraction (Yang, et al. *(29)*) are two common methods employed for object segmentation. The automatic threshold segmentation method iteratively selects a best threshold and then separates targeted particles based on the derived threshold value (McHugh, et al. *(30)*). The advantage of this method is its implementation simplicity when only one image is used. However, two main problems are encountered when applying threshold-based segmentation:

1. *Low efficiency*: The background in on-line images changes continuously because of variations in illumination or fluid transparency. Thus, an automatic threshold algorithm is required for each image for debris tracking. This process greatly increases the processing time and makes it unsuitable for use in on-line monitoring.
2. *Low accuracy*: Some inherent image characteristics, such as blurring, reduce the contrast between the wear debris and the background. Therefore, some backgrounds are incorrectly recognized as wear particles. Such a misidentification by the threshold method is illustrated in Fig. 4. Some background areas enclosed by red lines are incorrectly identified as wear particles.

The purpose of background subtraction is to identify targets using a preselected image, the so-called background image (Su, et al. *(31)*). Wear particles can thus be separated by subtracting the background. It is advantageous to use a series of sampled images to reconstruct a background image closest to the current background. In this work, the Surendra background updating algorithm (Zeng, et al. *(32)*) was modified and employed for
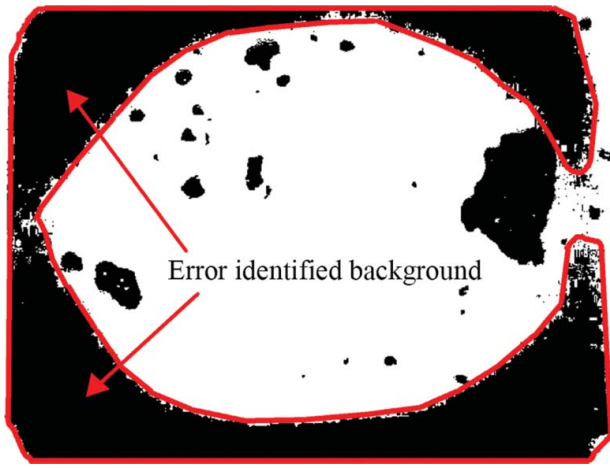
Figure 4. Wear debris segmentation result of Fig. 2a with an automatic threshold method.

background reconstruction of on-line images. A four-step procedure is given below.

1. Store the first frame image, $I_0(x, y)$, from the sampled video.
2. Preprocess the frame $I_0(x, y)$ to acquire an approximate background image $B_0(x, y)$, and then assign $I_0(x, y) = B_0(x, y)$.
3. Calculate the difference image $D_i(x, y)$ between the current ith frame $I_i(x, y)$ and the previous frame $I_{i-1}(x, y)$ and transform the difference image to a binary image with a predefined threshold τ_1 according to the gray level distribution. That is,

$$D_i(x, y) = \begin{cases} 1, & |I_i(x, y) - I_{i-1}(x, y)| \geq \tau_1 \\ 0, & \text{otherwise} \end{cases}, \quad [1]$$

where, $i = 1, 2, \ldots, N_{max}$; N_{max} is the total number of video frames.

1. 4. Update the background image $B_i(x, y)$ based on the binary difference image $D_i(x, y)$ according to

$$B_i(x, y) = \begin{cases} B_{i-1}(x, y), & D_i(x, y) = 1 \\ \alpha I_i(x, y) + (1 - \alpha)B_{i-1}(x, y), & D_i(x, y) = 0 \end{cases}, \quad [2]$$

where $B_i(x, y)$ becomes the current background image and α is a weighting factor in the range [0, 1]. Considering the fact that the background would not change abruptly, the value of α is conservatively set to 0.9. $B_i(x, y)$ can thus be regarded as the real-time background image of the ith frame.

In step 2, a preprocessing operation is employed to remove the wear debris in the first frame image shown in Fig. 5a. Hence, the time taken for background reconstruction process is significantly reduced. The gray value of any pixel is denoted as $N \in [0, 255]$ and the average gray value of pixels in a row is denoted as M. If $|N - M| > \mu$ (where μ is the deviation and set to 10), then set $N = M$. After processing all pixels with the above procedure, an approximate background image is obtained with decreased gray contrast.

The processed result is shown in Fig. 5b. It can be seen that all wear particles were removed. Based on this, a real-time background was constructed dynamically with steps 3 and 4, and an example result using a series of 400 frames from the sampled video is shown in Fig. 5c. The image displays a high similarity with the average background shown in these on-line images.

Wear debris segmentation

With a well-reconstructed background (see the final reference image in Fig. 5c), wear debris in subsequent frames can be segmented using the following procedures. First, the background intensity is subtracted from a new frame containing wear debris. Second, the resultant image is processed with binary transformation and denoising; that is,

$$S_{i+1}(x, y) = \begin{cases} 0, & |I_{i+1}(x, y) - B_i(x, y)| > \tau_2 \\ 255, & \text{otherwise} \end{cases}, \quad [3]$$

where S_{i+1} denotes the segmented image after binarization of the new image I_{i+1}; τ_2 is a threshold that can be computed by
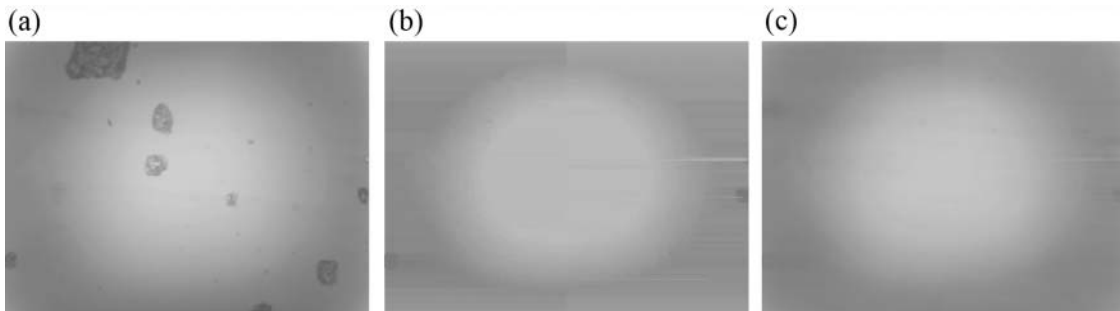
(a) (b) (c)

Figure 5. Dynamic background reconstruction of a series of on-line ferrograph frame images: (a) initial image, (b) reference image after preprocessing, and (c) final background image.
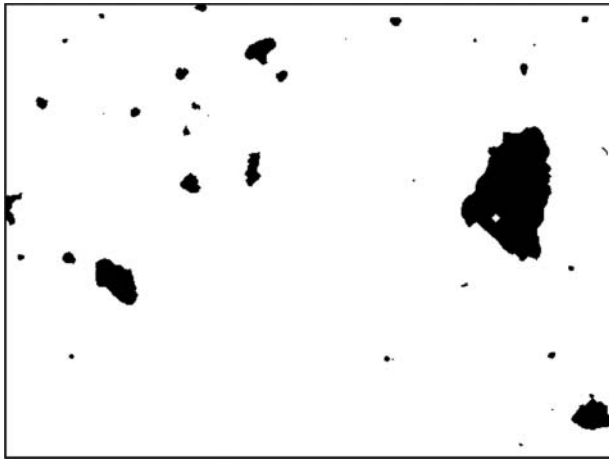
Figure 6. Segmentation result of Fig. 2a using the background difference method.

using Otsu's method (Otsu *(33)*). Finally, the output image is obtained and illustrated in Fig. 6, from which it can be seen that the wear particles are well segmented.

The background subtraction method has distinct advantages in wear debris segmentation. It is able to maintain the wear debris contour integrity and suppress noise residuals in the image. Furthermore, the algorithm is self-adaptive to luminance variation in on-line wear debris images.

Dynamic tracking of moving wear debris

Due to the rotation and translation motion, wear particles always show different appearances in different frames. Therefore, it is necessary to track wear debris in individual frames. In addition, having multiple wear particles in one image imposes a challenge in distinguishing individual wear debris. There are various methods for dynamic tracking of moving objects, such as mean shift (Mazinan and Amir-Latifi *(34)*), Kalman filter (Fu and Han *(35)*), and kernel-based object tracking (Yao, et al. *(36)*). In this work, a centroid tracking method is adopted to track wear debris by considering the following points:

1. A centroid is a point in the image having a statistical average property and thus remains unchanged even when the shape of wear debris changes.
2. A centroid is calculated based on a binary image; its validity is independent of the original gray image.
3. Within the target area, defects such as holes or fractures have little influence on the centroid value.

The centroid (x_c, y_c) of each identified wear debris is calculated separately using

$$x_c = \frac{\sum x_i}{N_p}, \quad y_c = \frac{\sum y_i}{N_p}, \quad i = 0,\ 1,\ ...,\ N_p, \qquad [4]$$

where x_i and y_i are coordinates of pixels segmented as a debris patch, and N_p is the number of pixels in the patch.

It is observed that the same particle is often imaged in two sequential frames. The maximum distance moved can be calculated based on the controlled fluid flow rate and the exposure time, which is used to define the radius of a detected circle. By doing this, the same particle can be identified by searching for the nearest centroid in two adjacent frames. The radius is very small due to the short exposure time. If new particles appear within the detected circle, they would be considered a larger particles. Then the particle area changes significantly. In this case, the adhesion particle is easily examined and its tracking procedure will be stopped. Figure 7 shows an example of single particle tracking, in which a large particle is identified and then tracked. Furthermore, multiparticle tracking is accomplished by extending the single-objective tracking algorithm described above.

Feature construction based on multiview images

A multiview image contains more morphological information than a single-view 2D image. This allows for spatial morphological features to be constructed based on the ASTM International Standard (F1877-05 *(37)*) guidance for wear particle classification using the extracted 2D features. Basically, four 2D morphological features, including major dimension (*L*), minor dimension (*W*), area (*A*), and perimeter (*P*), can be extracted from each single-view image. By using these fundamental parameters, three indicators specific to wear debris identification are calculated as follows:

1. Aspect ratio (*AR*): *AR* is the length-to-width ratio of wear debris. It is applied to describe cutting wear debris.

$$AR = \frac{L}{W} \qquad [5]$$

2. Equivalent circle diameter (*ECD*): *ECD* is defined as the diameter of a circle with an area equivalent to the area of
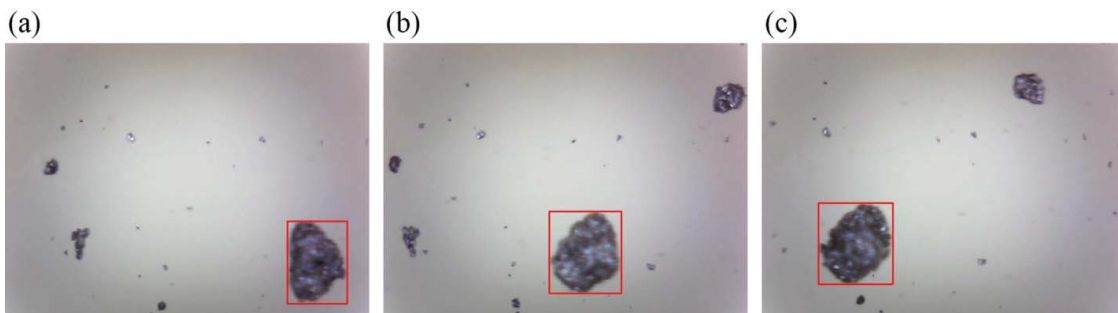

Figure 7. (a)–(c) Three images selected from the result of single-particle tracking.

the wear debris and has the unit of length. It is used to denote the size of irregular wear debris.

$$ECD = \sqrt{\frac{4A}{\pi}} \qquad [6]$$

3. Roundness (R): R refers to the shape of a particle with regard to a circle. Roundness varies from zero to one in magnitude, with a perfect circle having a value of 1.

$$R = \frac{4A}{\pi L^2} \qquad [7]$$

Extracting spatial morphological parameters from 2D images has been reported in other works (Mora and Kwan (38)), in which thickness was found to be correlated linearly with the projection area with a 2D view. Such a rough approximation is acceptable when only single-view images are available. In contrast, multiview images provide the shape and surface information of wear debris in different views. Thus, it is possible to extract and reconstruct spatial morphological features. For example, particle thickness (T) can be set equal to the minimum value of all minor dimensions of multiple images captured from different directions. Hence, three spatial indicators can be constructed as follows:

1. Spatial diameter (SD): SD is the maximum value of all ECD values in multiview images. It reflects a spherical equivalent diameter regardless of particle shape and roughness. That is,

$$SD = \max\{ECD\} \qquad [8]$$

2. Height aspect ratio (HAR): HAR is the ratio of the maximum dimension and thickness, which is employed to distinguish laminar particles because they have a large surface area but with a small thickness.

$$HAR = \frac{L_{max}}{T} \qquad [9]$$

Hence, laminar particles have a greater HAR value than other types including fatigue chunks and severe sliding particles (Peng, et al. (13)).

1. 3.Sphericity (S): S is the indicator of a spatial profile enclosing the particle and should be in the range [0, 1]. The larger the S value is, the more sphere-like the particle is. According to Mora and Kwan (38), sphericity is calculated as

$$S = \sqrt[3]{\frac{W_{max} T}{L_{max}^2}}, \qquad [10]$$

where W_{max} and L_{max} denote the two maximum values of all minor and major dimensions of multiview images.

Experiments and results

To evaluate the effectiveness of the proposed method, two experiments were carried out. The first one aimed at examining the advantages of the proposed multiview imaging method by inspecting individual moving particles. The second experiment was designed to examine debris characterization using multiple particles. Some particle samples were prepared with commercial iron powder in a sieve size of less than 150 μm and the others with a similar size were manually selected from the friction and wear tests. All lubricant samples were diluted with gear lube to simulate lubrication samples from a gearbox. Using iron powder with a known size range and morphological information, the extracted particle features of this system could be compared and verified. The video of wear debris was sampled using the dynamic wear debris image acquisition system, with a sampling rate of 50 fps in true color format and a resolution of 640 × 480 (width × height) pixels. Different views of moving wear debris were captured and indexed before their features were extracted by applying dynamic object detection and tracking.

Experiment with single wear particle

To demonstrate that the developed system is able to image different types of wear particles with various features, three typical wear particles, including sphere-, flake-, and fiber-like shapes, were captured and their 2D and spatial morphological features were extracted using a series of multiview images. The different views of these three types of particles are shown in Figs. 8–10, respectively. It can be found in these figures that the wear particles show different contours in different images due to their physical motion.

Four basic and six constructed parameters were extracted with each image and categorized as shown in Tables 1–3. In addition, three newly constructed spatial parameters were adopted to determine the types of particles.

The spatial features, described by the proposed parameters, are able to provide additional information for wear particle identification. It can be concluded from Tables 1–3 that the spatial parameters can well characterize particle types as designated. For example, the sphericity of a sphere-like particle (Fig. 8) has a high value of 0.84, which indicates a high spherical approximation. Similarly, a fiber-like particle, shown in Fig. 10, has a high value of the height aspect ratio. Therefore, the proposed spatial parameters can be adopted to distinguish these typical wear particle types.

In addition to wear types, particle dimension is important for wear condition characterization (Wu, et al. (39)). Therefore, a dimensional parameter, spatial diameter, can be used to indicate any changes in the wear condition. With the spatial parameters on size (T, SD) and shape (S, HAR) features, a comprehensive characterization of wear condition can be accomplished (Williams (40)).
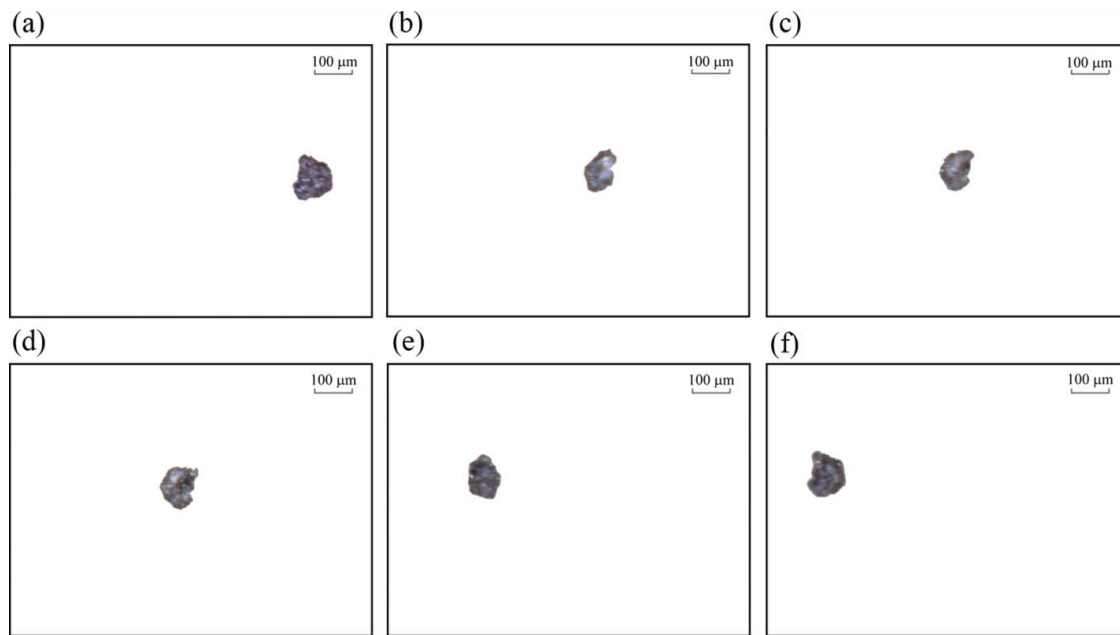
Figure 8. (a)–(f) Image frames acquired from the video of a moving sphere-like particle.

Experiment with multiple wear particles

In practice, a large amount of wear particles are produced continuously during a wear process. A series of image frames were extracted from the sampled video, as shown in Fig. 11, to illustrate this phenomenon. Multiple particles can be analyzed at the same time by utilizing the video acquisition and image processing system.

The constructed spatial parameters together with the maximum values of the basic parameters were calculated to evaluate the diversity of the particles, as shown in Table 4. It is observed that most 2D parameters, such as L_{max}, W_{max}, and A_{max}, had a large value range, which means that the imaged particles are different in size. The variations in shape features, such as S and HAR, are smaller than that of dimension features including T and SD, as shown in Table 4. As mentioned above, S and HAR can be used to identify the sphere-like and fiber-like particles. Most particles captured in this experiment are close to a sphere; thus, the variation in sphericity is very small. However, the height aspect ratio parameter, HAR, shows a slightly larger variation than that of S. This is because the shape of debris No. 7 is irregular in comparison to others, as shown in Figs. 11b–11d, resulting in its HAR (2.97) being much larger than others. These results demonstrate that 3D morphological information extracted using the proposed approach makes wear debris characterization and identification more reliable than that based on
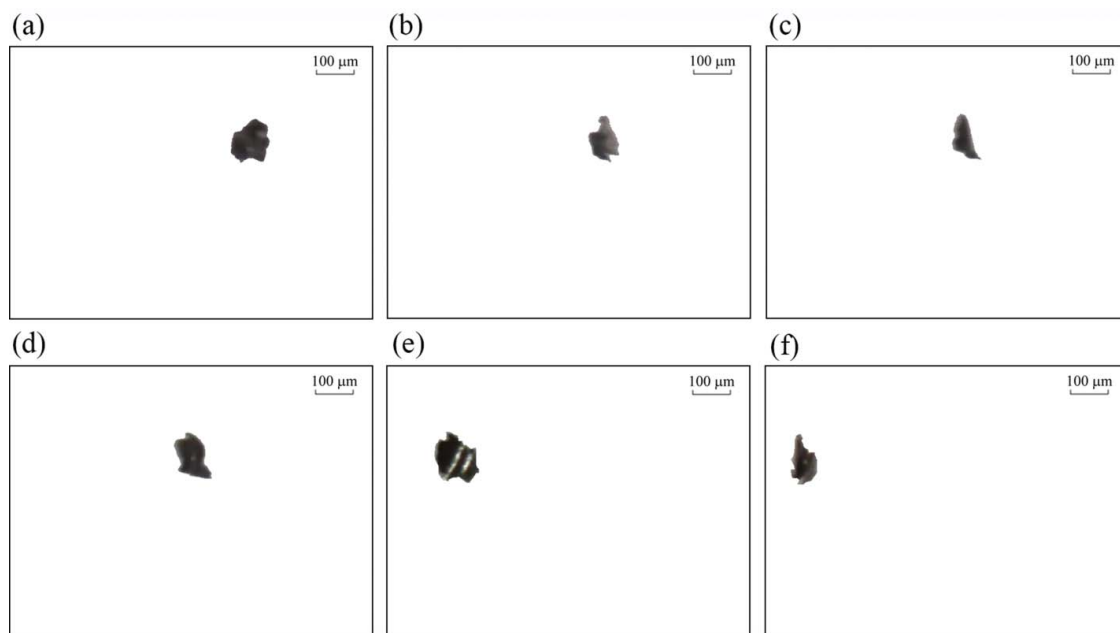

Figure 9. (a)–(f) Image frames acquired from the video of a moving flake-like particle.
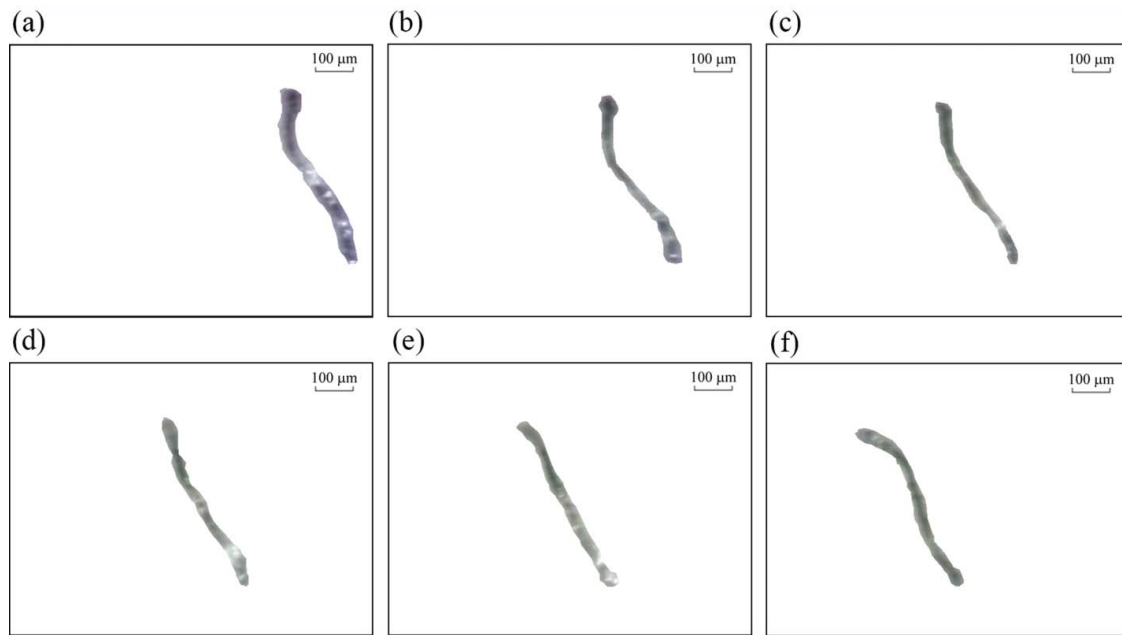
Figure 10. (a)–(f) Image frames acquired from the video of a moving fiber-like particle.

Table 1. Parameters of the sphere-like wear debris extracted from multiview images in Fig. 8.

| | Basic parameters | | | | | | | Constructed parameters | | | |
| | Two-dimensional | | | | | | | Three-dimensional | | | |
Image	L (μm)	W (μm)	A (μm^2)	P (μm)	AR	ECD (μm)	R	T (μm)	SD (μm)	S	HAR
(a)	123.42	114.50	3,961.37	261.71	1.08	71.02	0.33	80.30	71.02	0.84	1.56
(b)	121.93	80.30	2,911.55	227.51	1.52	60.89	0.25				
€	123.42	83.27	3,015.64	231.97	1.48	61.96	0.25				
(d)	120.45	99.63	3,487.02	251.30	1.21	66.63	0.31				
(e)	123.42	90.71	3,284.78	233.46	1.36	64.67	0.27				
(f)	124.91	111.53	3,909.32	255.76	1.12	70.55	0.32				

Table 2. Parameters of the flake-like wear debris extracted from multiview images in Fig. 9.

| | Basic parameters | | | | | | | Constructed parameters | | | |
| | Two-dimensional | | | | | | | Three-dimensional | | | |
Image	L (μm)	W (μm)	A (μm^2)	P (μm)	AR	ECD (μm)	R	T (μm)	SD (μm)	S	HAR
(a)	114.50	101.12	3,616.38	255.76	1.13	67.86	0.35	52.05	76.33	0.65	2.77
(b)	121.93	71.38	2,554.67	248.33	1.71	57.03	0.22				
(c)	129.37	52.05	2,075.85	227.51	2.49	51.41	0.16				
(d)	135.32	86.25	3,287.76	261.71	1.57	64.70	0.23				
(e)	144.24	108.55	4,575.50	309.30	1.33	76.33	0.28				
(f)	133.83	69.89	2,447.60	248.33	1.91	55.82	0.17				

Table 3. Parameters of the fiber-like wear debris extracted from multiview images in Fig. 10.

| | Basic parameters | | | | | | | Constructed parameters | | | |
| | Two-dimensional | | | | | | | Three-dimensional | | | |
Image	L (μm)	W (μm)	A (μm^2)	P (μm)	AR	ECD (μm)	R	T (μm)	SD (μm)	S	HAR
(a)	502.61	53.53	9,134.64	767.29	9.39	107.85	0.05	35.69	107.85	0.20	14.08
(b)	486.25	47.58	6,618.64	747.96	10.22	91.80	0.04				
(c)	475.84	35.69	5,485.54	706.33	13.33	83.57	0.03				
(d)	495.17	37.18	6,014.92	734.58	13.32	87.51	0.03				
(e)	495.17	38.66	6,465.48	749.45	12.81	90.73	0.03				
(f)	489.22	35.69	6,463.99	762.83	13.71	90.72	0.03				

Table 4. Parameters of all captured wear debris in Fig. 11.

	Basic parameters						Constructed parameters			
	Two-dimensional						Three-dimensional			
Wear debris number	L_{max} (μm)	W_{max} (μm)	A_{max} (μm^2)	P_{max} (μm)	AR_{max}	R_{max}	T (μm)	SD (μm)	S	HAR
1	89.22	63.94	1,692.21	166.54	1.39	0.27	53.28	46.41	0.73	1.82
2	62.45	53.53	1,147.96	136.80	1.17	0.37	48.43	38.23	0.80	1.70
3	87.73	59.48	2,081.80	184.39	1.47	0.34	52.48	51.49	0.77	1.47
4	66.92	52.05	1,460.23	150.19	1.29	0.41	48.58	43.12	0.73	2.03
5	44.61	31.23	575.47	93.68	1.42	0.38	24.02	27.06	0.72	1.91
6	101.12	65.43	2,023.81	215.62	1.53	0.25	60.75	50.76	0.70	1.87
7	86.25	38.66	1,009.67	160.60	2.21	0.17	30.18	35.86	0.53	2.97
8	220.08	163.57	12,150.28	452.05	1.35	0.32	142.50	124.38	0.78	1.58
9	104.09	65.43	2,334.59	200.75	1.60	0.27	54.96	54.53	0.68	1.96
10	115.99	102.60	3,347.24	249.82	1.13	0.32	96.09	65.28	0.80	1.73
11	83.27	56.51	1,424.55	166.54	1.48	0.26	52.90	42.60	0.72	1.84

2D features only. More significant, a large amount of particles can be sampled in on-line monitoring of a running machine, and the statistical distribution of wear debris can be provided for reliable condition monitoring.

Discussion

It is difficult to obtain 3D characteristics for on-line wear debris analysis because spatial information cannot be extracted from 2D images. At present, there are two on-line systems similar to the one described in this work. They are on-line visual ferrography (Wu, et al. (41)) and LaserNet Fines (Spectro Inc. (22)). However, these systems possess some limitations compared to the system developed in this work. The on-line visual ferrograph sensor uses magnetic force to attract wear debris in fluid flow to a plane surface to capture particle images. This results in chain patterns of wear debris and it is difficult to extract features of individ-
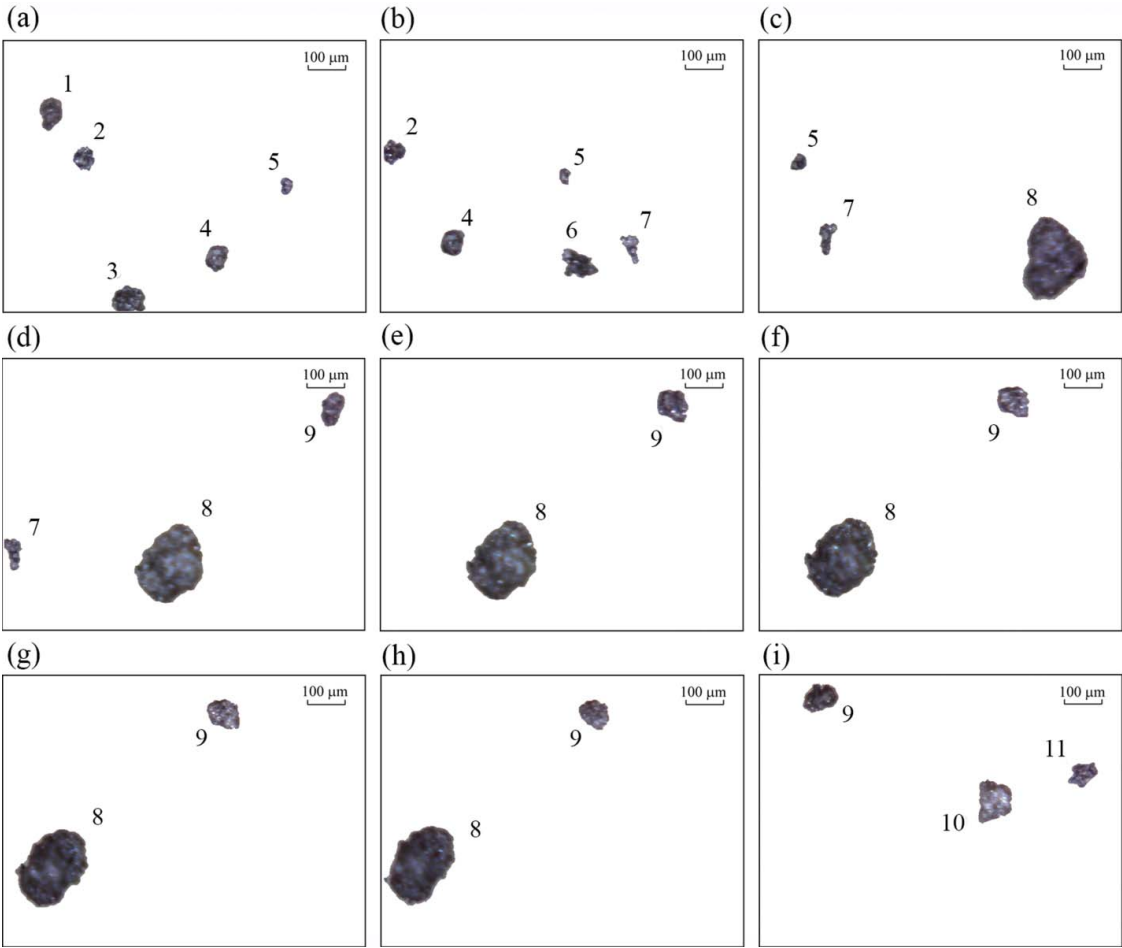

Figure 11. (a)–(i) Series of selected frames with multiple wear particles sampled from a manual fluid sample in a time span of 16 s.

ual particles. Moreover, the LaserNet Fines system only provides particle information from a single view and imposes challenges in extracting 3D features. On the other hand, multiview images are able to provide spatial morphological information on both 2D and 3D characterization features. More significant, 3D morphological information extracted using the proposed approach makes it more reliable for wear debris identification. The particle size and shape, together with the particle concentration as a wear rate indicator, can reflect wear condition stages as well as the evolution of machine wear states. In order to improve the multiview method, accuracy of analysis can be increased by employing a larger set of imaged wear particles in terms of acquiring the video in a higher frame rate.

It should be mentioned that wear debris images are directly captured from lubricating fluid; thus, the transparency of a lubricant is one of the key points to obtaining clear images. Therefore, the proposed method is mainly suitable for gearbox condition monitoring because the transparency of gearbox fluid is higher than that of some other machines; for example, diesel engines. This is why all experimental particles are simulated to be gearbox lubricating samples. Though the lubricant fluid samples are manually prepared, the presented 3D feature extraction approach still has potential value in engineering applications when the system is connected to a gearbox lubricant circuit.

Conclusion

This article has presented a method to detect dynamic particles in different views to obtain 3D features for on-line wear monitoring. A video acquisition system was used to capture dynamic images of rotating particles in the form of multiview images. The particles in different image frames were successfully identified by making use of an integration of background subtraction and centroid tracking. Experimental results demonstrated that there is a high variation in particle features, which leads to the conclusion that multiview images are able to provide more reliable and comprehensive information of wear debris than a single-view image in terms of their spatial morphology.

Funding

References

(1) Kumar, M., Mukherjee, P. S., and Misra, N. M. (2013), "Advancement and Current Status of Wear Debris Analysis for Machine Condition Monitoring: a Review," *Industrial Lubrication and Tribology*, **65**(1), pp 3–11.

(2) Wu, T., Wang, J., Peng, Y., and Zhang, Y. (2012), "Description of Wear Debris from On-Line Ferrograph Images by Their Statistical Color," *Tribology Transactions*, **55**(5), pp 606–614.

(3) Wang, J., and Wang, X. (2013), "A Wear Particle Identification Method by Combining Principal Component Analysis and Grey Relational Analysis," *Wear*, **304**(1/2), pp 96–102.

(4) Zhang, Y., Mao, J., and Xie, Y. (2011), "Engine Wear Monitoring with OLVF," *Tribology Transactions*, **54**(2), pp 201–207.

(5) Wang, J., Yao, P., Liu, W., and Wang, X. (2015), "A Hybrid Method for the Segmentation of a Ferrograph Image Using Marker-Controlled Watershed and Grey Clustering," *Tribology Transactions*, **59**(3), pp 513–521.

(6) Li, Z., Yan, X., Guo, Z., Liu, P., Yuan, C., and Peng, Z. (2012), "A New Intelligent Fusion Method of Multi-Dimensional Sensors and Its Application to Tribo-System Fault Diagnosis of Marine Diesel Engines," *Tribology Letters*, **47**(1), pp 1–15.

(7) Yuan, C., Peng, Z., and Yan, X. (2005), "Surface Characterization Using Wavelet Theory and Confocal Laser Scanning Microscopy," *Journal of Tribology*, **127**(2), pp 394–404.

(8) Stachowiak, G., and Podsiadlo, P. (2008), "3-D Characterization, Optimization, and Classification of Textured Surfaces," *Tribology Letters*, **32**(1), pp 13–21.

(9) Tian, Y., Wang, J., Peng, Z., and Jiang, X. (2012), "A New Approach to Numerical Characterisation of Wear Particle Surfaces in Three-Dimensions for Wear Study," *Wear*, **282–283**, pp 59–68.

(10) Yuan, C., Peng, Z. X., Yan, X., and Zhou, X. (2008), "Surface Roughness Evolutions in Sliding Wear Process," *Wear*, **265**(3/4), pp 341–348.

(11) Podsiadlo, P., and Stachowiak, G. W. (2012), "Directional Multiscale Analysis and Optimization for Surface Textures," *Tribology Letters*, **49**(1), pp 179–191.

(12) Stachowiak, G. P., Stachowiak, G. W., and Podsiadlo, P. (2008), "Automated Classification of Wear Particles Based on Their Surface Texture and Shape Features," *Tribology International*, **41**(1), pp 34–43.

(13) Peng, Z., Kirk, T. B., and Xu, Z. L. (1997), "The Development of Three-Dimensional Imaging Techniques of Wear Particle Analysis," *Wear*, **203–204**, pp 418–424.

(14) Peng, Z., and Tomovich, S. (2008), "The Development of a New Image Acquisition & Analysis System for 3D Surface Measurements Using Confocal Laser Scanning Microscopy," *Advanced Materials Research*, **32**, pp 173–179.

(15) Wang, M., Peng, Z., Vasilev, K., and Ketheesan, N. (2013), "Investigation of Wear Particles Generated in Human Knee Joints Using Atomic Force Microscopy," *Tribology Letters*, **51**(1), pp 161–170.

(16) Du, L., and Zhe, J. (2011), "A High Throughput Inductive Pulse Sensor for Online Fluid Debris Monitoring," *Tribology International*, **44**(2), pp 175–179.

(17) Feng, S., Che, Y., Mao, J., and Xie, Y. (2014), "Assessment of Anti-wear Properties of Lube Fluids Using Online Visual Ferrograph Method," *Tribology Transactions*, **57**(2), pp 336–344.

(18) Cao, W., Chen, W., Dong, G., Wu, J., and Xie, Y. (2014), "Wear Condition Monitoring and Working Pattern Recognition of Piston Rings and Cylinder Liners Using On-Line Visual Ferrograph," *Tribology Transactions*, **57**(4), pp 690–699.

(19) Murali, S., Xia, X., Jagtiani, A. V., Carletta, J., and Zhe, J. (2009), "Capacitive Coulter Counting: Detection of Metal Wear Particles in Llubricant Using a Microfluidic Device," *Smart Materials and Structures*, **18**(3), pp 1–6.

(20) Filicky, D., Sebok, T., Lukas, M., and Anderson, D. (2002), "LaserNet Fines—A New Tool for the Fluid Analysis Toolbox." Available at: http://www.machinerylubrication.com/Read/383/lasernet-fines-fluid-analysis (accessed September 8, 2015).

(21) Wu, T., Peng, Y., Sheng, C., and Wu, J. (2014), "Intelligent Identification of Wear Mechanism via On-Line Ferrograph Images," *Chinese Journal of Mechanical Engineering*, **27**(2), pp 411–417.

(22) Spectro Inc. (2013), "Lasernet Fines Q200—A Solution to Fluid Analysis Including Particle Count and Particle Shape Classification." Available at: http://landing.spectroinc.com/default/assets/File/January2014/Q200_WPv2_2013-08-10.pdf (accessed September 8, 2015).

(23) Dan, R. M. (2013), *Multi-View and Three-Dimensional (3D) Images in Wear Debris Analysis (WDA)*, Doctoral Thesis, University of Manchester, School of Mechanical, Aerospace and Civil Engineering: Manchester, UK.

(24) Peng, Y., Wu, T., Wang, S., and Peng, Z. (2015), "Oxidation Wear Monitoring Based on the Color Extraction of On-Line Wear Debris," *Wear*, **332–333**, pp 1151–1157.

(25) Peng, Y., Wu, T., Wang, S., Kwok, N. M., and Peng, Z. (2015), "Motion-Blurred Particle Image Restoration for On-Line Wear Monitoring," *Sensors*, **15**(4), pp 8173–8191.

(26) Meijering, E., Dzyubachyk, O., and Smal, I. (2012), "Methods for Cell and Particle Tracking," *Methods in Enzymology*, **504**(9), pp 183–200.

(27) Karasulu, B., and Korukoglu, S. (2012), "Moving Object Detection and Tracking by Using Annealed Background Subtraction Method in Videos: Performance Optimization," *Expert Systems with Applications*, **39**(1), pp 33–43.

(28) Zhang, J., Liang, J., and Zhao, H. (2013), "Local Energy Pattern for Texture Classification Using Self-Adaptive Quantization Thresholds," *IEEE Transactions on Image Processing*, **22**(1), pp 31–42.

(29) Yang, J., Shi, M., and Yi, Q. (2012), "A New Method for Motion Target Detection by Background Subtraction and Update," *Physics Procedia*, **33**, pp 1768–1775.

(30) McHugh, J. M., Konrad, J., Saligrama, V., and Jodoin, P. M. (2009), "Foreground-Adaptive Background Subtraction," *IEEE Signal Processing Letters*, **16**(5), pp 390–393.

(31) Su, F., Fang, G., and Kwok, N. M. (2012), "Adaptive Colour Feature Identification in Image for Object Tracking," *Mathematical Problems in Engineering*, **2012**, pp 1–18.

(32) Zeng, Y., Lan, J., Ran, B., Gao, J., and Zou, J. (2015), "A Novel Abandoned Object Detection System Based on Three-Dimensional Image Information," *Sensors*, **15**(3), pp 6885–6904.

(33) Otsu, N. (1979), "A Threshold Selection Method from Gray-Level Histograms," *IEEE Transactions on Systems, Man, and Cybernetics*, **9**(1), pp 62–66.

(34) Mazinan, A. H., and Amir-Latifi, A. (2012), "Improvement of Mean Shift Tracking Performance Using a Convex Kernel Function and Extracting Motion Information," *Computers & Electrical Engineering*, **38**(6), pp 1595–1615.

(35) Fu, Z., and Han, Y. (2012), "Centroid Weighted Kalman Filter for Visual Object Tracking," *Measurement*, **45**(4), pp 650–655.

(36) Yao, A., Lin, X., Wang, G., and Yu, S. (2012), "A Compact Association of Particle Filtering and Kernel Based Object Tracking," *Pattern Recognition*, **45**(7), pp 2584–2597.

(37) F1877-05. (2010), "Standard Practice for Characterization of Particles," ASTM International: West Conshohocken, PA.

(38) Mora, C. F., and Kwan, A. K. H. (2000), "Sphericity, Shape Factor, and Convexity Measurement of Coarse," *Cement and Concrete Research*, **30**(3), pp 351–358.

(39) Wu, T., Peng, Y., Du, Y., and Wang, J. (2014), "Dimensional Description of On-Line Wear Debris Images for Wear Characterization," *Chinese Journal of Mechanical Engineering*, **27**(6), pp 1280–1286.

(40) Williams, J. A. (2005), "Wear and Wear Particles—Some Fundamentals," *Tribology International*, **38**(10), pp 863–870.

(41) Wu, T., Mao, J., Wang, J., Wu, J., and Xie, Y. (2009), "A New On-Line Visual Ferrograph," *Tribology Transactions*, **52**(5), pp 623–631.